 doi:10.20944/preprints202112.0397.v1

*Article*

# Axial Force Analysis of the Support Bracket of Pumped Storage Unit

**Buchao Xu [1], Weiqiang Zhao [2], Wenhua Lin [1], Zhongyu Mao [2], Ran Tao [2], Zhengwei Wang [2,*]**

[1] Fujian Xianyou Pumped Storage Co. Ltd., Xianyou, Fujian Province, 351267, China
[2] State Key Laboratory of Hydroscience and Engineering & Department of Energy and Power Engineering, Tsinghua University, Beijing, 100084, China
* Correspondence: wzw@mail.tsinghua.eud.cn; Tel.: +86 13601363209

**Abstract:** During operation, the support bracket is the main part to withstand the axial loads of the pumped storage unit. Moreover, the effects of axial loads including the hydraulic thrust of runner flow and the weight of runner body may cause the support bracket deformation and fatigue damage. For the safe and stable operation, the simulation of the axial force and the structural analysis of the support bracket of a pumped storage unit was carried out in this paper. The CFD simulation result has revealed the variation rule of the axial force in different operating conditions. Using ANSYS Mechanical, the static stresses and deformation of support bracket with axial loads were calculated. The results release the location and variations of maximum stress and maximum deformation caused by the axial loads. By comparing the predicted maximum axial force with the admission force calculated by the structural analysis, it is found that the axial force of the researched machine is within the safe range. This study provides the reference for the safety and stable operation of the pumped storage unit.

**Keywords:** pump-turbine; support bracket; runner axial force; stress; deformation

## 1. Introduction

Pumped storage is a kind of energy that can consume excessive energy when the generation is larger than the consumption and provide energy to the grid when the supply is not enough. Till today, pumped storage is the only large energy that can balance the energy in the power grid [1]. In recent decades, pumped storage units developed rapidly in the worldwide for its pivotal role in the electric systems [2]. With the develop of the new renewable energies such as wind and solar energy, the supply to the power grid becomes more and more intermittent because of the unstable weather and alternate of day and night [3,4]. With the new condition, the pumped storage units start and stop within very short time frequently to meet the requirements of both generating mode and pump mode [5]. Because of the special design, pump-turbine units have to withstand more hydraulic excitations than the other types of hydraulic turbines. During operation, the support bracket is the main part to withstand the axial loads of the whole unit. The axial loads include the hydraulic thrust of runner flow and the weight of runner body, typically up to millions of tons in general [6]. The overload in axial direction may cause the support bracket deformation and fatigue damage which lead to the runner move down and even be unconducive to the operation stability. Therefore, it is important to have deeper research on the support bracket of pumped storage units in order to analyse the consequence of the axial forces on the structure and avoid serious damage and fatigue.

Theoretical analysis of the axial force of hydraulic machinery is the most commonly used method in engineering [7]. Xiangyang Li, Zhongyu Mao, et. al simulated the load-rejection process of a pump-turbine unit. The CFD calculation have considered the full leakage in runner crown and shroud. The research found that the pressure difference between crown leakage and internal-runner near outlet is the key factor in inducing axial

Preprints (www.preprints.org) | NOT PEER-REVIEWED | Posted: 24 December 2021 doi:10.20944/preprints202112.0397.v1

force [8]. Jinwei Li, Yuning Zhang, et. al quantitatively investigated the hydraulic force on the impeller of a pump turbine through CFD and found that both the amplitude of the force and its dominant components strongly depend on the operating conditions [9]. With the gradual improvement of computer performance and the continuous improvement of computational fluid dynamics (CFD) technology, CFD has become an important method for studying the flow characteristics of units [10] and axial force characteristics [11]. On the basis of axial force analysis theory and gap modeling, many researchers further apply CFD to the research and analysis of hydraulic machinery axial force. Shi Weidong et al. found through CFD simulation that the axial force on the inner surface of the runner accounts for a large proportion of the hydraulic mechanical axial force, which is the most important factor affecting the axial force [12]. Zhou et al. found through CFD simulation that the axial force on the inner surface of the runner is restricted by hydraulic design, and balancing the pressure difference between the gap between the front and rear cover plates of the impeller is the main method and feasible way to adjust the axial force of the hydraulic machinery [13].

Many researchers have focused on the structure characteristics of pumped storage units. Tanaka investigated the runner dynamic stress and vibration due to hydraulic excitation forces in both experimental and theoretical aspects. The relationship between runner vibration and the interaction of runner blades and guide vanes was revealed [14]. Egusquiza et al. monitored the vibration of several pumped storage units in 15 years and analyzed the vibration evolution of units. They found damage in the generator, in bearings, in supporting structures caused by vibration and presented the damage would change the vibration of units interactively [15]. The vibrations of the upper and lower brackets and the top cover were all measured for three water heads in Zhang et al.'s study. It found that the vibration of top cover is more sensitive to the variation of water head than the upper and lower brackets [16]. In numerical simulation, He et al. studied the stresses and deformation of pump turbine runner based on the one-way fluid structure interaction method. The maximum stress locations are always at the fillets of blade leading edges near the band [17,18]. However, there are relatively few historical studies in the area of structure characteristic of support brackets, let alone the axial force simulation on the pump turbine units. In this paper, the stresses and deformation of support bracket with a certain range axial load are analyzed based on ANSYS. In addition, the characteristics of the axial force will be analysed based on the computational fluid dynamics (CFD) method. This study will be helpful to predict the structure characteristic of support brackets and enhance the operation stability of pumped storage unit.

## 2. Method and Model

### *2.1 The structure analysis method*

The structural motion equation for a linear structural system can be written as [19,20]:

$$\boldsymbol{M_s}\{\ddot{u}\} + \boldsymbol{C_s}\{\dot{u}\} + \boldsymbol{K_s}\{u\} = \{F_s\} \tag{1}$$

where $\boldsymbol{M_s}$ is the mass matrix, $\boldsymbol{C_s}$ is the damping matrix, $\boldsymbol{K_s}$ is the stiffness matrix, $\{u\}$, $\{\dot{u}\}$, $\{\ddot{u}\}$ is the vectors of node deformation, velocity and acceleration, $\{F_s\}$ is the vectors of force loaded on structure.

The static stress $\sigma$ can be calculated by:

$$\sigma = \boldsymbol{D_s B_s}\{u\} \tag{2}$$

where $\boldsymbol{D_s}$ is the elastic matrix and $\boldsymbol{B_s}$ is the strain-displacement matrix.

The equivalent von Mises stress $\sigma_c$ can be calculated using the fourth strength theory:

$$\sigma_c = \sqrt{\frac{1}{2}[(\sigma_1 - \sigma_2)^2 + (\sigma_2 - \sigma_3)^2 + (\sigma_3 - \sigma_1)^2]} \tag{3}$$

where $\sigma_1$, $\sigma_2$ and $\sigma_3$ are the first, second and third principal stress.

Preprints (www.preprints.org) | NOT PEER-REVIEWED | Posted: 24 December 2021 doi:10.20944/preprints202112.0397.v1

*2.2 The CFD simulation method*

This study uses CFD numerical simulation as a method to carry out the simulation and analysis of the internal flow of the pump-turbine. Based on the Reynolds Time Average (RANS) method, the continuity equation, momentum equation, and energy equation can be written as the following equations:

$$\frac{\partial \overline{u_i}}{\partial x_i} = 0 \tag{4}$$

$$\rho \frac{\partial \overline{u_i}}{\partial t} + \rho \overline{u_j} \frac{\partial \overline{u_i}}{\partial x_j} = \frac{\partial}{\partial x_j}\left[-\bar{p}\delta_{ij} + 2\mu \overline{S_{ij}} - \rho \overline{u_i u_j'}\right] \tag{5}$$

$$\frac{\partial}{\partial t}(\rho h_{tot}) - \frac{\partial p}{\partial t} + \frac{\partial}{\partial x_j}(\rho u_j h_{tot}) = \frac{\partial}{\partial x_j}\left(\lambda_t \frac{\partial T}{\partial x_j} - \overline{u_j h_{sta}}\right) + \frac{\partial}{\partial x_j}\left[u_j\left(2\mu \overline{S_{ij}} - \rho \overline{u_i u_j'}\right)\right] \tag{6}$$

Where, $u$ represents the velocity, $t$ represents the time, $\rho$ represents density, $x$ is the component of the coordinate system, $\delta_{ij}$ is the Kroneker number, $\mu$ is the dynamic viscosity, $\rho \overline{u_i u_j'}$ is the Reynold stress, $\overline{S_{ij}}$ is the averaged strain rate tensor, $T$ is temperature, $h_{sta}$ is the static enthalpy, $h_{tot}$ is the total enthalpy and $\lambda_t$ is the thermal conductivity coefficient.

Because of the disclosure of Reynolds Time Average simulation equation, turbulence model is required to be introduced to close the equation. Based on Boussinesq assumption, vortex viscosity coefficient $\mu_t$ is defined. The tensor relation between Raynold stress and averaged strain rate tensor is built up as following:

$$-\rho u_i' u_j' = 2\mu_t S_{ij} - \frac{2}{3} k \delta_{ij} \tag{7}$$

In this equation, k is the turbulence kinetic energy. In this research, the SST k-ω model is used as the turbulence model [21,22]. By combination the standard k-ε model and Wilcox k-ω model, the adaptation of k-ω model is increased and it will be able to solve the strong reverse pressure gradient flow and strong boundary layer shear flow. The turbulent kinetic energy $k$ equation and the dissipation rate $\omega$ equation are as follows:

$$\frac{\partial(\rho k)}{\partial t} + \frac{\partial(\rho u_i k)}{\partial x_i} = P - \frac{\rho k^{\frac{3}{2}}}{l_{k-\omega}} + \frac{\partial}{\partial x_i}\left[(\mu + \sigma_k \mu_t)\frac{\partial k}{\partial x_i}\right] \tag{8}$$

$$\frac{\partial(\rho \omega)}{\partial t} + \frac{\partial(\rho u_i \omega)}{\partial x_i} = C_\omega P - \beta \rho \omega^2 + \frac{\partial}{\partial x_i}\left[(\mu_l + \sigma_\omega \mu_t)\frac{\partial \omega}{\partial x_i}\right] + 2(1 - F_1)\frac{\rho \sigma_{\omega 2}}{\omega}\frac{\partial k}{\partial x_i}\frac{\partial \omega}{\partial x_i} \tag{9}$$

Where, $P$ is turbulence generation term, $F_1$ is the mixing equation, $\sigma_k$, $\sigma_\omega$, $\beta_k$ and $C_\omega$ are model coefficients, and $l_{k\text{-}\omega}$ is the turbulence scale, which can be calculated by $l_{k\text{-}\omega}=k^{1/2}\beta_k\omega$.

## 3. Model and simulation settings

*3.1 Model of CFD*

3.1.1 Meshing

Preprints (www.preprints.org) | NOT PEER-REVIEWED | Posted: 24 December 2021 doi:10.20944/preprints202112.0397.v1

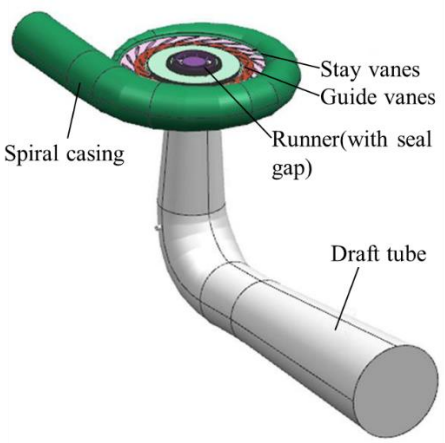


**Figure 1.** Flow passage model of pump-turbine

Before CFD simulation, the calculation domain needs to be meshed. The grid is divided by a structured/unstructured unit hybrid grid structure. Structured grid is used in the geometrically regular area in order to save the storage space and improve computing and addressing capabilities. The unstructured grids are used in geometrically irregular areas to improve geometric adaptability and grid quality, and enhance computational convergence.

In this study, the calculation domains of draft tube, runner and its seal and gap, movable guide vane, fixed guide vane, and volute were separately meshed. Because the runner and its seal and gap have a significant influence on the calculation of the axial force, the grid of the runner and its seal and gap is particularly refined. The number of grid nodes is determined after the GCI grid convergence checking [20], as shown in Table 1.

**Table 1** Mesh node number of all the components

| Component | Number of the nodes |
|---|---|
| Draft tube | 348822 |
| Runner | 3663918 |
| Runner seal and gap | 5894860 |
| Guide vane | 1957000 |
| Stay vane | 834840 |
| Spiral casing | 301592 |
| Total | 13001032 |

3.1.2 Simulation configuration

Based on the fluid domain as shown in Figure 1, the flow is calculated under pump conditions. The fluid flows from the draft tube and flows out from the spiral casing. Therefore, the boundary conditions are given as follows: 1) The draft tube inlet is given as a speed inlet, and the speed value depends on the discharge; 2) Pressure outlet is given to the spiral casing outlet, and the average value is set. The pressure is 1 Atm; 3) All wall boundaries are set as non-slip wall surfaces; 4) Each part is connected by a junction surface model.

The steady-state calculation is the first step of the calculation. The maximum number of iterations is set as 600, and the convergence criterion is that the residual error between the momentum equation and the continuity equation is less than $1\times10^{-5}$. Base on steady-state calculation results, transient calculations are performed. There are 360 time steps in each cycle of the runner and the maximum number of iterations per time step is 10 to ensure convergence. The convergence criterion is still the equation residual between the momentum equation and continuity is less than $1\times10^{-5}$. In steady-state calculations and transient calculations, the discrete format of the convective term of the momentum

Preprints (www.preprints.org) | NOT PEER-REVIEWED | Posted: 24 December 2021 doi:10.20944/preprints202112.0397.v1

equation is set to high precision, and the discrete format of the convective term of the turbulent transport equation is set to the first order.

*3.2 Model of the structure*

The researched case is the model of the structure of a support bracket of a pumped storage unit in China shown in Figure 2. The diameter of the basic support part is 4 m while the diameter with eight supporting arms is 10 m. The end of eight arms were fixed by the concrete foundation and the bottom were connected with the generator stator. In the simulation, the end of supporting arms and the bottom were set as fixed support. In the pumped storage unit, the axial loads including the hydraulic thrust of runner flow and the weight of runner are loaded on the thrust bearing. In this study, the axial loads were set as a certain range value and loaded on the bushes of thrust bearing uniformly. The material density of support bracket is 7.75 kg/m$^3$. The Young's modulus is 2.1×10$^{11}$ Pa. The Poisson's ratio is 0.3.

Tetrahedral meshes were used for the structure model meshing shown in Fig. 2. Since stress concentrations often occur at the corner of support plates, the fillet of the plates were modeled accurately. The mesh at these sensitive areas were refined to avoid stress concentrations due to the mesh. To meet the criteria for mesh independence check, the final meshes used in this study have 0.55 million nodes and 0.3 million elements.

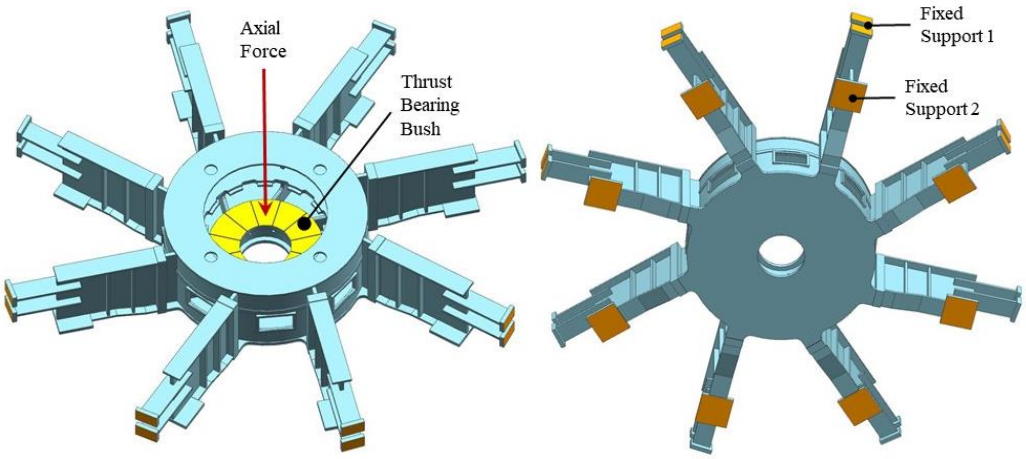


**Figure 2**. The three-dimensional model of the support bracket

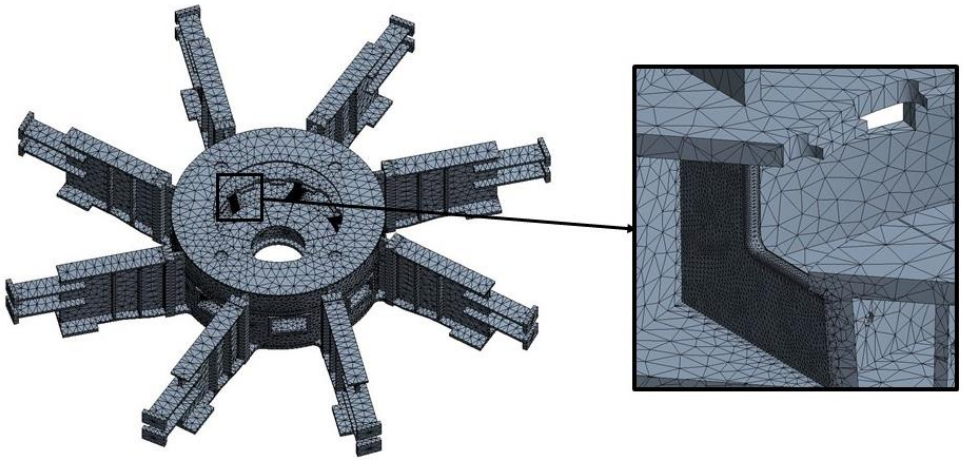

**Figure 3**. The calculation model of the support bracket

## 4. Results and Discussion

*4.1 Axial force prediction*

Preprints (www.preprints.org) | NOT PEER-REVIEWED | Posted: 24 December 2021 doi:10.20944/preprints202112.0397.v1

The variation of the axial force of the unit with the discharge coefficient $C_\varphi$ predicted by CFD (the negative value means the downward axial force) is shown in Figure 4, where the direction of the axial force is downward. Based on the figure, it can be seen that basically the absolute value of the downward axial force on the runner decreases with the increase of the flow rate while it increases a little when the discharge is large. In addition, when the discharge is low, the axial force decreases significantly to around $1.4\times10^5$ N.

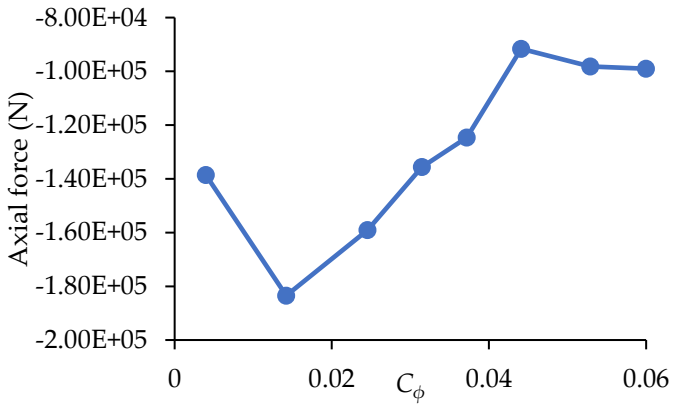


**Figure 4** Variation of runner axial force with flow rate

The causes of the axial force on the runner will be analysed here. The meridional map of runner, including the crown and band gap, is shown in Figure 5. The reason for the axial force on the runner is relatively complicated. The main causes come from the pressure difference between the crown gap and the runner, and the pressure difference between the band gap and the runner. According to the division of areas #1 and #2 in the figure, it can be seen that in area #1, the pressure of the crown gap is $p_{c1}$, the pressure of the adjacent position of the runner is $p_{c2}$, the pressure of the band gap is ps1, and the pressure of the adjacent position of the runner is $p_{s2}$. Usually, $p_{c1}\approx p_{s1}$ and $p_{c2}\approx p_{s2}$. Therefore, $p_{c1}$-$p_{c2}\approx p_{s1}$-$p_{s2}$, that is, the axial force of the runner in the #1 area is balanced. On the contrary, in #2 area, the pressure $p_{c3}$ in the crown gap and the pressure $p_{c4}$ adjacent to the runner are difficult to balance, causing the runner to receive upward or downward axial force.

In the pump condition, the lower the discharge is, the larger the head is, as well as the outlet pressure of the runner. At this moment, the guide vane opening is small, which confines the high-pressure fluid in the runner side. The high pressure in the crown gap makes $p_{c3}>>p_{c4}$, which increases the down-ward axial force.

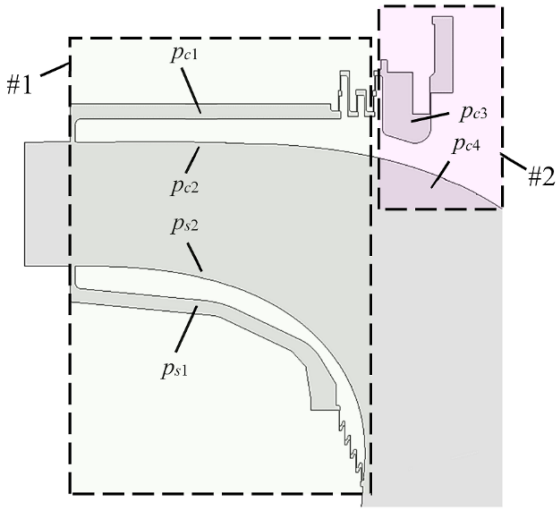


**Figure 5** Meridional map of runner with indication of hub and crown leakages

Preprints (www.preprints.org) | NOT PEER-REVIEWED | Posted: 24 December 2021 doi:10.20944/preprints202112.0397.v1

*4.2 Influence of axial force on the support bracket*

Based on the FEM method in ANSYS, the stresses and deformation of support bracket with axial load on thrust bearing bushes were analyzed. The axial loads are from $5\times10^6$ N to $2\times10^7$ N [3][4]. For the sake of brevity, the axial force loaded on thrust bearing will be referred by the abbreviations 'AF' in below. Since the distribution rules of equivalent stress and deformation are uniform with different AF, Figure 6 and Figure 7 only show the distribution at AF = $1\times10^7$ N to explanation.

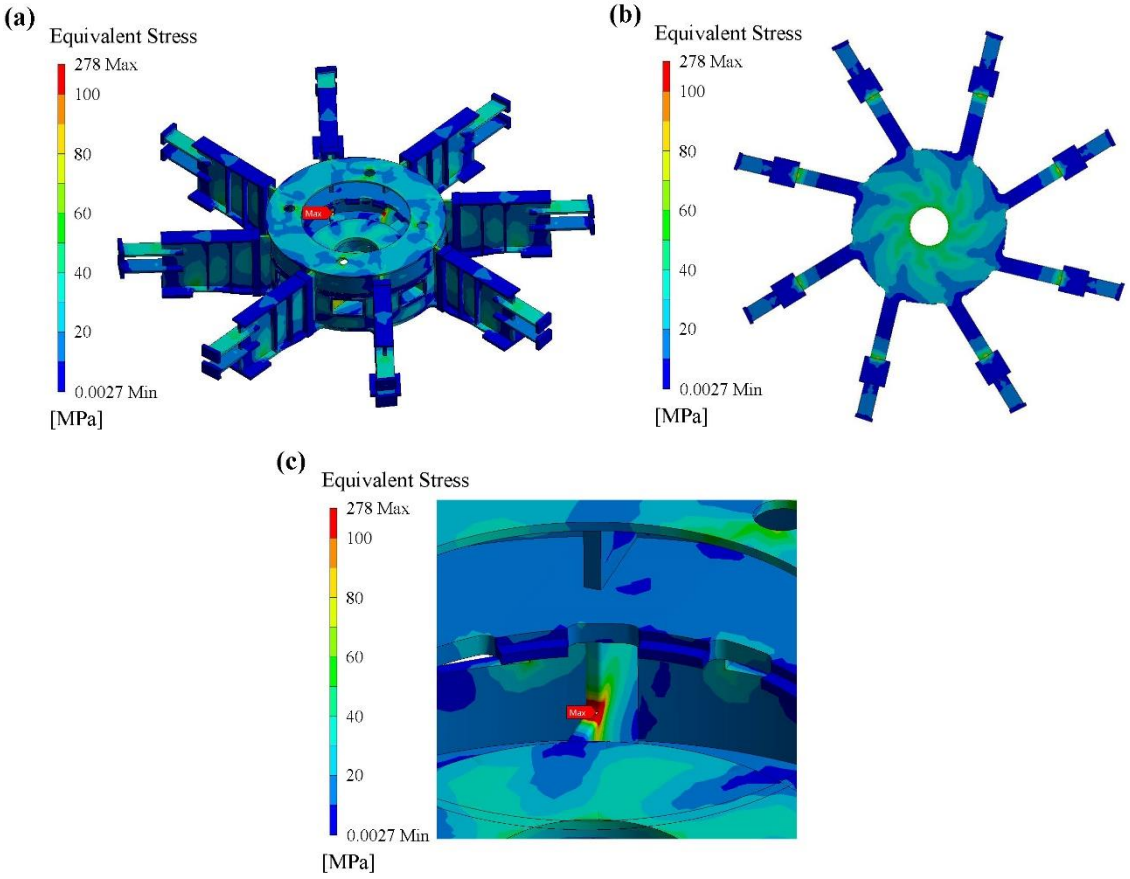


**Figure 6** The equivalent stress distribution of support bracket at AF = $1\times10^7$N

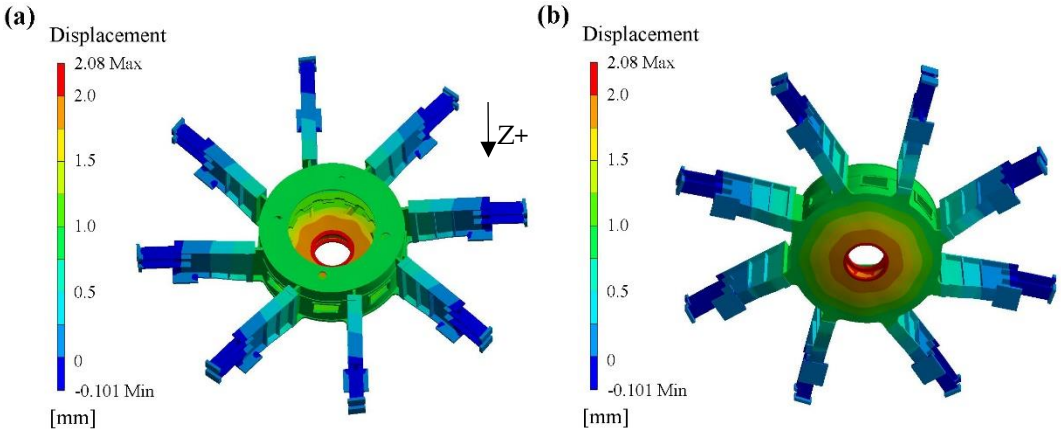


**Figure 7** The axial displacement distribution of support bracket at AF = $1\times10^7$N

As can be seen from the Figure 6, the maximum stresses often concentrate on the corner of support plates. When the AF reaches to $1.0\times10^7$ N, the maximum stresses on support bracket have been up to 278 MPa. From the displacement distribution, we can see that the maximum axial deformation is around 2 mm in this case and the location is on

Preprints (www.preprints.org) | NOT PEER-REVIEWED | Posted: 24 December 2021 doi:10.20944/preprints202112.0397.v1

the inner circle of thrust bearing. The deformation gradually decreases as the radius increases since the end of support arms are fixed. Interestingly, there is tiny upward deformation between the 2 fixed locations of support arms.

Figure 8 provides the variation of the maximum equivalent stress and the maximum deformation in support bracket with different AF loaded on thrust bearing. The results indicate that the maximum equivalent stress and the maximum deformation changed linearly with the AF. While the AF= $5\times10^6$ N, the maximum stress is 125 MPa and the maximum deformation is 1mm. However, while the AF exceeds around $1.25\times10^7$ N, the maximum stress is exceeded the admissible stress of Q345, which might cause structure yield and deformation. Meanwhile the maximum deformation exceeds around 2.5 mm, which would lead to the runner move down and the gap in crown and band change. This result can provide reference for the design of pumped storage units, especially the structure design of support bracket and hydraulic design of pumped storage turbine. According to Figure 4,the maximum axial force imposed on the runner is $1.83\times10^5$ N, which is far lower than the admission force of $1.25\times10^7$ N. In this case, the bracket is in safe condition in all of the operating conditions.

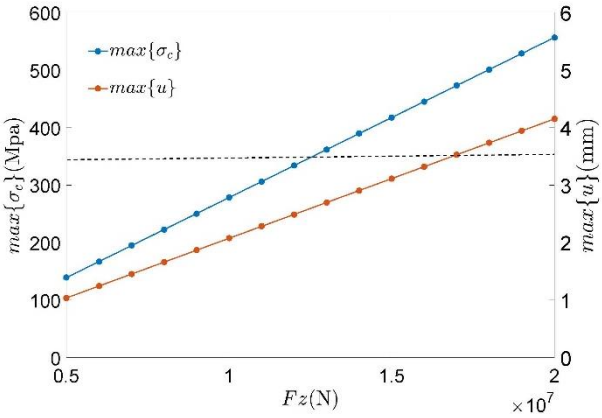


**Figure 8** Variation of the maximum equivalent stress and the maximum deformation in support bracket with different AF

## 5. Conclusions

In this investigation, the aim was to discuss the influence of axial force on the structural characteristics of support bracket of pumped storage unit by means of CFD and FEM. Firstly, the fluid domain of a pump-turbine is built and the axial force is simulated. Then the FEM is applied on the structure of the bracket. The location of the maximum equivalent stress and the maximum deformation are found. In the end, the simulated axial force is compared with the admission force of the structure. This research should be helpful for improving predictions of the impact of axial load on support bracket and the whole pumped storage units. The main results are:

1. The computational fluid dynamics method in this case has considered the gap between the upper crown and the lower ring of the runner, which can effectively predict the axial force characteristics of the runner and provide a theoretical basis for the safe and stable operation of the pump turbine unit. Gap modeling will increase the computational cost, but it provides a solution to the problem of axial force.
2. Under the pump mode, the pump turbine is subject to strong axial force. Especially when the flow rate and the guide vane opening is small and the head is high, the downward axial force is relatively large, which will cause safety hazards to the support bracket. The axial force in pump turbine is mainly caused by the pressure imbalance between the upper and lower gaps and the runner.
3. The maximum stresses often concentrate on the corner of support plates and the largest deformation occurs on the location of thrust bearing. While the axial loads exceed

1.25×10$^7$ N, the stress on the corner of support plates would exceed the admissible stress, causing bracket downward deformation and leading to the runner move down and the gap in crown and band change. The predicted maximum axial force is 1.83×10$^5$ N, which is within the admission force range.

**Author Contributions:** Conceptualization, Buchao Xu; methodology, Weiqiang Zhao; software, Wenhua Lin; validation, Ran Tao; investigation, Weiqiang Zhao; resources, Buchao Xu; data curation, X.X.; writing—original draft preparation, Zhongyu Mao and Weiqiang Zhao; writing—review and editing, Weiqiang Zhao; visualization, Zhongyu Mao; supervision, Zhengwei Wang; project administration, Zhengwei Wang; funding acquisition, Buchao Xu. All authors have read and agreed to the published version of the manuscript.

**Funding:** This research was funded by National Natural Science Foundation of China (No.: 51876099).

**Data Availability Statement:** Not applicable.

**Acknowledgments:** Thanks for the test data provided by relevant units and the support of National Natural Science Foundation of China (No.: 51876099).

**Conflicts of Interest:** The authors declare no conflict of interest.

## References

1. Zhao, W.; Egusquiza, M.; Valero, C.; Valentín, D.; Presas, A.; Egusquiza, E. On the Use of Artificial Neural Networks for Condition Monitoring of Pump-Turbines with Extended Operation. *Measurement* **2020**, *163*, 107952, doi:10.1016/j.measurement.2020.107952.
2. Rehman, S.; Al-Hadhrami, L.M.; Alam, M.M. Pumped Hydro Energy Storage System: A Technological Review. *Renewable and Sustainable Energy Reviews* **2015**, *44*, 586–598.
3. International Energy Agency *World Energy Outlook 2020*; Paris, 2020;
4. International Energy Agency *Global Energy Review 2020*; Paris, 2020;
5. Zhang, Y.; Zhang, Y.; Wu, Y. A Review of Rotating Stall in Reversible Pump Turbine. *Proceedings of the Institution of Mechanical Engineers, Part C: Journal of Mechanical Engineering Science* **2017**, *231*, 1181–1204.
6. Li Wan; Wei Wang; Haijun Gao; Rangqin Gong; Zhongdong Qian Numerical Research of Axial Hydraulic Thrust of Runner in Baihetan Hydropower Station. *China Rural Water and Hydropower* **2014**, *12*, 161–164.
7. Norton, T.; Sun, D.-W. Computational Fluid Dynamics (CFD)–an Effective and Efficient Design and Analysis Tool for the Food Industry: A Review. *Trends in Food Science & Technology* **2006**, *17*, 600–620.
8. Li, X.; Mao, Z.; Lin, W.; Bi, H.; Tao, R.; Wang, Z. Prediction and Analysis of the Axial Force of Pump-Turbine during Load-Rejection Process. In Proceedings of the IOP Conference Series: Earth and Environmental Science; IOP Publishing, 2020; Vol. 440, p. 052081.
9. Li, J.; Zhang, Y.; Liu, K.; Xian, H.; Yu, J. Numerical Simulation of Hydraulic Force on the Impeller of Reversible Pump Turbines in Generating Mode. *Journal of Hydrodynamics, Ser. B* **2017**, *29*, 603–609.
10. Tao, R.; Xiao, R.; Liu, W. Investigation of the Flow Characteristics in a Main Nuclear Power Plant Pump with Eccentric Impeller. *Nuclear Engineering and Design* **2018**, *327*, 70–81.
11. Anderson, D.; Tannehill, J.C.; Pletcher, R.H. *Computational Fluid Mechanics and Heat Transfer*; Taylor & Francis, 2016; ISBN 1466578300.
12. SHI Weidong; LI Qifeng; LU Weigang; Zhang Desheng Estimation and Experiment of Axial Thrust in Centrifugal Pump Based on CFD. *Transactions of the Chinese Society for Agricultural Machinery* **2009**, *40*, 60–63.
13. Zhou, L.; Shi, W.; Li, W.; Agarwal, R. Numerical and Experimental Study of Axial Force and Hydraulic Performance in a Deep-Well Centrifugal Pump with Different Impeller Rear Shroud Radius. *Journal of Fluids Engineering* **2013**, *135*.
14. Tanaka, H. Vibration Behavior and Dynamic Stress of Runners of Very High Head Reversible Pump-Turbines. *International Journal of Fluid Machinery and Systems* **2011**, *4*, 289–306, doi:10.5293/IJFMS.2011.4.2.289.
15. Egusquiza, E.; Valero, C.; Valentin, D.; Presas, A.; Rodriguez, C.G. Condition Monitoring of Pump-Turbines. New Challenges. *Measurement* **2015**, *67*, 151–163, doi:10.1016/j.measurement.2015.01.004.
16. Zhang, Y.; Zheng, X.; Li, J.; Du, X. Experimental Study on the Vibrational Performance and Its Physical Origins of a Prototype Reversible Pump Turbine in the Pumped Hydro Energy Storage Power Station. *Renewable energy* **2019**, *130*, 667–676.
17. He, L.Y.; Wang, Z.W.; Kurosawa, S.; Nakahara, Y. Resonance Investigation of Pump-Turbine during Startup Process. In Proceedings of the IOP Conference Series: Earth and Environmental Science; IOP Publishing, 2014; Vol. 22, p. 032024.

18. He, L.; Zhou, L.; Ahn, S.-H.; Wang, Z.; Nakahara, Y.; Kurosawa, S. Evaluation of Gap Influence on the Dynamic Response Behavior of Pump-Turbine Runner. *Engineering Computations* **2019**.
19. Xiao, R.; Wang, Z.; Luo, Y. Dynamic Stresses in a Francis Turbine Runner Based on Fluid-Structure Interaction Analysis. *Tsinghua Science and Technology* **2008**, *13*, 587–592.
20. Clough, R.W.; Penzien, J. *DYNAMIQUE DES STRUCTURES-TOME 1-PRINCIPES FONDAMENTAUX*; 1980; ISBN 2862160016.
21. Menter, F.R.; Kuntz, M.; Langtry, R. Ten Years of Industrial Experience with the SST Turbulence Model. *Turbulence, heat and mass transfer* **2003**, *4*, 625–632.
22. Menter, F. Zonal Two Equation Kw Turbulence Models for Aerodynamic Flows. In Proceedings of the 23rd fluid dynamics, plasmadynamics, and lasers conference; 1993; p. 2906.